

Crystalline crosslinked microparticles from immiscible blends of polyethylene and polystyrene

Gerald H. Ling^a, Montgomery T. Shaw^{a,b,*}

^a Polymer Program, Institute of Materials Science, University of Connecticut, 97 North Eagleville Road, Storrs, CT 06269, USA

^b Chemical, Materials, and Biomolecular Engineering, University of Connecticut, Storrs, CT 06269, USA

ARTICLE INFO

Article history:

Received 29 April 2009

Received in revised form

29 July 2009

Accepted 1 August 2009

Available online 7 August 2009

Keywords:

Microgels

Crosslinked crystalline polyethylene microparticles

Immiscible blends

ABSTRACT

Crystalline crosslinked polyethylene microparticles with size distribution averages ranging from 0.374 to 0.944 μm were prepared from immiscible PS and PE blends in the melt phase for microgel applications. The particles were crosslinked either concurrently while blending using dicumyl peroxide or post blending via electron-beam irradiation. The effects of varying the processing temperature, blend duration, and block copolymer compatibilizer content on the particle morphology were studied and it was found that only a decrease in processing temperatures (increase in continuous-to-dispersed phase viscosity ratio) resulted in finer particles for the range of variables tested. The chemical composition of the isolated particles was determined using infrared and nuclear magnetic resonance spectroscopy while the particle morphology was investigated using electron microscopy image analysis in conjunction with thermogravimetric analysis. It was determined that particles produced with and without the block copolymer contained a small amount of PS even after meticulous extraction with a PS solvent (THF). However, the exact location of PS on the PE particles remains obscure.

© 2009 Elsevier Ltd. All rights reserved.

1. Introduction

Microgels comprise swollen intermolecularly crosslinked macromolecules suspended in a fluid, which is often a solvent for the polymer from which the microgel is formed [1,2]. The degree to which most microgels swell and de-swell in their suspending fluid depends on the crosslink density and the solvent interaction with the polymer [3]. The latter is a function of temperature and hence, most microgels possess the ability to change size and occasionally, shape as the temperature of the system varies. This attribute can prove useful in industry as the microgels can be used as an additive to alter the viscosity of fluids by varying the particle volume fraction with temperature as the particles swell and contract. However, the change in size due to changes in temperature is typically small, especially in situations where highly crosslinked microgels are required. This in turn limits the useful application range of such microgels as viscosity modifiers except in high concentrations, where the change in volume fraction at such concentrations would be large enough to cause a significant change in the viscosity due to impingement.

In response to this matter, we have proposed a microgel of relatively high crosslink density with a crystalline core that is capable of swelling up to two times its original size when heated beyond the melting temperature of the crystalline core [4]. These crystalline microgels were developed using a top-down approach whereby crosslinked PE from high-voltage cable insulation was mechanically fragmented. However, this process resulted in microgels with highly irregular shapes that also led to unexpected interparticle interactions [5]. Also, the fixed crosslinked density of the recycled PE was limiting.

The goal of the work presented within describes a method of producing similar microgels with a range of crosslink densities that are not only more uniform in shape, but smaller as well. This was achieved by using an immiscible blend of PE and PS with PE being the minor and dispersed phase. Additionally, with the addition of a block copolymer compatibilizer, the surface of the PE particles may be functionalized for use in thermo-responsive microgel suspensions. Previous work on suspensions of similar PE microgels in squalane uncovered anomalous thermo-rheological response under low strains, but the system would jam and exhibit a non-reversible response. The nature of this phenomenon was hypothesized to be due to interparticle interactions brought about by surface chains co-crystallizing to form a delicate three-dimensional network. To investigate this hypothesis, we required particles that either interact strongly with one another, or not interact at all. The

* Corresponding author. Chemical, Materials, and Biomolecular Engineering, University of Connecticut, Storrs, CT 06269, USA. Tel.: +1 860 486 3980; fax: +1 860 486 4745.

E-mail address: montgomery.shaw@uconn.edu (M.T. Shaw).

former might be achievable by having PS grafted on the surface of the PE microgels, which would microphase separate in squalane and form interparticle links leading to a permanently jammed system, or exclude all interaction, depending upon the molecular weight of the PS block and its degree of swelling by the squalane.

By controlling the interfacial energy and shear-stress, extremely high capillary numbers, **Ca** can be reached resulting in micro- and nanoparticles, which when crosslinked, may be recovered for use as microgels that meet the above-mentioned criteria [6,7]. The usual expression for **Ca** is:

$$\mathbf{Ca} = \frac{\eta_m \dot{\gamma} D}{2\Gamma} \quad (1)$$

where:

$\dot{\gamma}$ is the shear rate

η_m is the viscosity of the continuous phase

D is the diameter of the dispersed spheres

Γ is the interfacial energy between the two phases

Although the dimensionless **Ca** was first used to help understand morphological developments in Newtonian-fluid mixtures at low Reynold's numbers (**Re** \rightarrow 0), it can in some cases help explain basic morphological changes in shear flow of non-Newtonian systems. Milliken and Leal, Mighri and Carreau, and Vickner et al. have looked into the effect of viscoelasticity on the morphology of droplets under shear flow and found that droplet deformation decreases with increasing droplet elasticity while matrix elasticity has an inverse effect [8,9,10]. In addition to that, the droplet breakup time increases as the droplet-to-matrix elasticity ratio increases.

Droplet breakup is promoted by the viscous shear stress, $\dot{\gamma}\eta$ while the interfacial stress, Γ/D counteracts it, keeping the droplet in an equilibrium spherical shape [11,12]. Hence, low values of **Ca** would result in stable, slightly deformed spheres while **Ca** values larger than the critical capillary number, **Ca_c** would cause the spheres to become unstable and break into smaller droplets [13,14,15,16]. Based on experimental data obtained by Grace [15], de Bruijn proposed the following empirical relation [16,17]:

$$\log \mathbf{Ca}_c = -0.506 - 0.0994 \log \eta_r + 0.124 \log^2 \eta_r + \frac{0.115}{\log \eta_{r,c} - \log \eta_r} \quad (2)$$

where η_r is the viscosity ratio between the dispersed and matrix phase and $\eta_{r,c} = 4.08$ is the critical viscosity ratio above which droplet breakup does not occur. The critical viscosity ratio only applies to shear flow systems and has been attributed to the continuous rotation of the dispersed particles that are sufficiently viscous to act like solid particles [18]. Equation (2) suggests that the **Ca_c** would diverge when $\eta_r = 0$ or when $\eta_r = \eta_{r,c}$, implying that inviscid and highly viscous drops would be resistant to breakup by shear flow [7].

There has been considerable effort over the last 50 years in the field of polymer blends with most of the work concentrating on improving the mechanical properties and processability of commodity polymers [19,20,21,22,23,24,25,26]. For the most part, blends of polymers are immiscible, so their mechanical properties must be carefully tailored to achieve useful mechanical properties. Hence, it is important to understand the effects of processing conditions on the blend morphology in order to predict the mechanical properties of new blend formulations.

However, to the extent of our knowledge, only a few have attempted to use immiscible blends as a method for producing crystalline microgels or nanofibers by harvesting the crosslinked

dispersed phase via solvent extraction of the matrix phase [21,25,27]. Recently, new results have been reported that has bearing to our work. Wang and colleagues have managed to extract crystalline PE and iPP structures with controllable morphology and size from immiscible blends of cellulose acetate-butyrate (CAB) with PE and PP blends [28,29,30]. By varying the processing conditions and composition of the blend, they were able to prepare well-defined microspheres and nanofibrils with sunflower- and bamboo-like structures.

Others have also reported similar structures, but prepared via different means. Nalaskowski et al. prepared hydrophobic polymer microspheres ranging from 2 to 50 μm by means of phase separation of PE and fossil resin from glycerol [31]. Aida's group has managed to synthesize crystalline PE nanofibers via metallocene-catalyzed extrusion polymerization of linear PE within mesoporous silica [32]. Li et al. on the other hand have reported similar nanofibers prepared using a template melt extrusion process whereby molten polymer was passed through an anodic aluminum membrane [33]. Chase and associates electrospun polyethylene microfibers at high temperatures using *p*-xylene as a solvent with the addition of salts in order to achieve high solution conductivity [34].

2. Experimental

2.1. Materials

STYRON[®] 666D PS resin was obtained from Dow Chemical (Midland, MI), while Tuflin Plus[®] HSJ-7037, a linear low-density PE resin was obtained from Union Carbide Corporation (Danbury, CT). The styrene-ethylene/butylene-styrene block copolymer compatibilizer, Kraton[®] G-1650E and butylated hydroxytoluene (BHT) antioxidant, IONOL CP were obtained from Shell Chemical (Houston, TX). Dicumyl peroxide (DCP) was obtained from Aldrich (St. Louis, MO) and used as received.

2.2. Sample preparation

Two different methods were employed to obtain crosslinked PE particles to be used as microgels. While both methods consist of melt-blending PE in a matrix of PS, the procedures used to crosslink the PE phase of the blend differed. The first crosslinking method utilized an electron-beam post blending while the second was achieved via in-situ reactive melt blending with DCP as a radical generator. Fig. 1 summarizes the steps of each different method used in preparing the crosslinked PE particles.

2.2.1. Crosslinked PE particles from blends crosslinked via electron-beam radiation (methods I and II)

PS-PE blends were prepared using a Prep-Center Model D-71 (C.W. Brabender, South Hackensack, NJ) equipped with roller-style blades. Mixing bowls with 30- and 60-cc capacities were used depending on the desired mixing temperatures, as lower mixing temperatures (higher **Ca** values) were only attainable by using a smaller mixing charge with its more favorable heat-transfer characteristics. Unless otherwise stated, the PS-PE ratio of all blends was 9:1 and the mixing speed was set at 75 rpm, which corresponds to a shear rate of 86 s^{-1} [35]. The high 9:1 PS-PE ratio was chosen as lower PS-PE ratios tend to result in larger PE particles or even co-continuous phases, depending upon the mixing conditions and rheological properties of the components [36]. The mixing speed was close to the maximum of the instrument and was chosen since most of the droplet breakup was expected to occur in this shear rate region corresponding to a particle-size minima as predicted by Sundararaj and Macosko [37]. Table 1 summarizes the blending parameters for each sample. Post mixing,

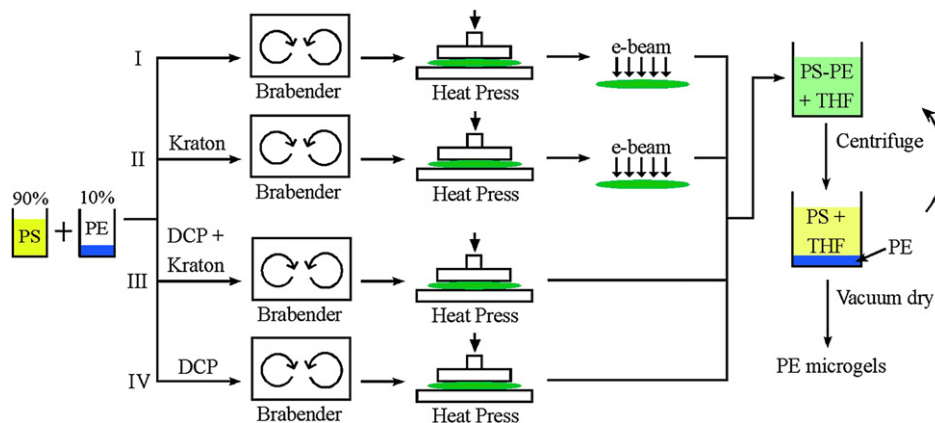


Fig. 1. Illustration of the different methods used in producing crosslinked PE particles from an immiscible PS–PE blend.

the blends were heat-pressed using a Model 2731 Laboratory Press (Carver, Wabash, IN) at 170 °C for 5 min into roughly 1-mm-thick sheets. These sheets were then exposed to 15 kGy of radiation from an electron beam, which resulted in a number-average molar mass (M_c) of 273 Da for the network chains of the PE particles. M_c was determined from the complex shear modulus, $|G^*|$ of neat PE strips that were prepared in the same manner as the PS–PE blends using the following equation:

$$M_c = \frac{\rho RT}{|G^*|} \quad (3)$$

where ρ is the density of PE, R is the ideal gas constant, and T is the absolute temperature. Following this, the sheets were dissolved in THF ($\rho = 0.88 \text{ g/cm}^3$ at 20 °C) and the resulting suspension was centrifuged for 30 min at 5000 rpm using an Avanti J-20 XP (Beckman Coulter, Fullerton, CA) centrifuge at 5 °C. The crosslinked PE particles were collected from the sediment, washed with fresh THF, and centrifuged again until the addition of methanol to the supernatant did not cause any precipitation, indicating that most of the unbound PS had been removed.

2.2.2. Crosslinked PE particles from blends crosslinked via peroxide (methods III and IV)

For the second method, a two-step technique similar to that described by Wang and colleagues [38] was used to prepare cross-linked PE particles. Neat PE was first melt blended with DCP and 0.01 wt% of BHT for 5 min at 140 °C to incorporate the peroxide for the subsequent step. The peroxide-infused PE was consequently melt blended with PS according to the same 9:1 PS–PE ratio and

5 wt% Kraton G[®] 1650 for 10 min at 150 °C and 75 rpm. The amount of BHT and Kraton G[®] 1650 added is based on the weight of PE in the blend. The addition of a small amount of sacrificial antioxidant (BHT) prevented “scorching” by scavenging radicals formed prematurely during the initial step, thus holding off the crosslinking reaction until the latter part of mixing process [39]. The blending parameters for samples prepared using this method are listed in Table 2. The resulting blends were then heat-pressed at 170 °C for 15 min into roughly 1-mm-thick sheets to drive the crosslinking process further towards completion. The half-lives of DCP in PE at 150 and 170 °C are 20 and 3 min respectively [40]. The crosslinked PE particles were recovered using the same technique as described in Section 2.2.1 whereby the PS matrix was washed with THF and particles separated from the liquid phase using centrifugation.

2.3. Fourier-transform infrared (FTIR) spectroscopy

FTIR experiments were conducted using a Nicolet Magna-IR 560 Spectrometer (Thermo Scientific, Waltham, MA). A total of 32 scans at a resolution of 4 cm^{-1} were run on samples pressed into films approximately 35- μm thick.

2.4. Scanning and transmission electron microscopy

Scanning electron microscopy (SEM) images were obtained using a JEOL 6335F Field Emission scanning electron microscope (JEOL, Japan), while transmission electron microscopy (TEM) images were obtained using a Philips EM 300 electron microscope (Eindhoven, The Netherlands). For SEM imaging, the PE particles were mounted on SEM support plates using carbon adhesive tape and sputter-coated with Au under vacuum prior to being imaged. For the TEM imaging, the PE particles were embedded in Spurr’s formulation [41] under vacuum and then cured at 60 °C over a period of two days. Once cured, the embedded PE particles were

Table 1

Blending parameters for 9:1 PS–PE blends prepared using the method outlined in Section 2.2.1.

Code	Kraton G [®] 1650, wt% ^a	Temperature, °C	Mixing time, min
0-175-10	0	175	10
5-175-10	5	175	10
10-175-10	10	175	10
5-175-20	5	175	20
0-150-10	0	150	10
5-150-10	5	150	10
10-150-10	10	150	10
5-150-20	5	150	20
0-125-10	0	125	10
5-125-10	5	125	10
10-125-10	10	125	10
5-125-20	5	125	20

^a The amount of block copolymer compatibilizer added is based on the weight of PE.

Table 2

DCP and Kraton G[®] 1650E content for the 9:1 PS–PE blends prepared using the method outlined in Section 2.2.2.

Code	DCP, wt% ^a	Kraton G [®] 1650, wt% ^a
DCP01K	0.1	5
DCP05K	0.5	5
DCP10K	1.0	5
DCP01	0.1	0
DCP05	0.5	0
DCP10	1.0	0

^a All additive amounts are based on PE.

microtomed using an Ultra 45° diamond knife (Diatome, Hatfield, PA). The microtomed sections were floated on water and picked up using a Formvar® support and dried. The sections were then exposed to OsO₄ vapors for 6 h before being imaged.

2.5. Nuclear magnetic resonance (NMR) spectroscopy

A Bruker DMX-500 MHz liquid-state NMR spectrometer (Billerica, MA) was used to record ¹H spectra using tetramethylsilane (TMS) as an internal reference. Chemical shifts are reported as ppm downfield from TMS. A total of 6800 scans with a delay of 3–5 s between scans were used for each sample. To dissolve or swell PS domains, samples were mixed with deuterated chloroform (CDCl₃) in 5-mm NMR tubes. The solid-state magic angle spinning ¹³C NMR experiments were collected on a Bruker DMX-300 MHz spectrometer operating at field strength of 7.05 T, hence a resonance frequency of 75.4 MHz for ¹³C. The samples were spun at 10 kHz and the chemical shifts were externally referenced to -CH₂ peak of adamantane at 38.2 ppm. The spectral width was 30 kHz with delay time of 20 s.

2.6. Thermogravimetric analysis (TGA)

Thermogravimetric experiments were carried out using a TA Instruments High-Res TGA 2950 (TA Instruments, New Castle, Delaware) with platinum sample holders. For all runs, argon flowing at 50 cc/min was used as a purge gas, and the heating rate was set at 5 °C/min from room temperature to 600 °C.

3. Results and discussion

3.1. Particle size distribution for PE particles produced using the method described in Section 2.2.1

The Weibull distribution function was fitted to the particle size data and the distribution parameters are listed in Table 3 along with the volume-average diameter of the particles, while Table 4 lists the corresponding viscosity ratios and capillary numbers. An example of the Weibull distribution function fitted using the particle size data of sample 0-150-10 is shown in Fig. 2. In general, all the PE particles prepared in this study fell within 0.1–1 μm, which agrees with results reported by Heindl et al. where 95:5 PS-PE blends prepared at 190 °C yielded PE particles with a volume-average size of 0.59 μm. A linear regression analysis on the factorial design

Table 3
Melt viscosity ratios and particle size data of extracted PE particles from blends prepared using the method outlined in Section 2.2.1.

Code ^a	Volume-average diameter, μm	Weibull distribution parameters, α; β
0-175-10	0.944 ± 0.003 ^b	0.933 ± 0.016 ^b ; 3.48 ± 0.26 ^b
5-175-10	0.805 ± 0.007	0.816 ± 0.005; 3.38 ± 0.10
10-175-10	0.860 ± 0.001	0.824 ± 0.013; 4.76 ± 0.50
5-175-20	0.808 ± 0.007	0.854 ± 0.009; 4.37 ± 0.37
0-150-10	0.979 ± 0.004	0.980 ± 0.007; 2.97 ± 0.12
5-150-10	0.848 ± 0.006	0.882 ± 0.007; 5.12 ± 0.35
10-150-10	0.556 ± 0.001	0.554 ± 0.004; 8.26 ± 0.69
5-150-20	0.501 ± 0.002	0.514 ± 0.004; 3.65 ± 0.15
0-125-10	0.374 ± 0.001	0.351 ± 0.004; 2.86 ± 0.13
5-125-10	0.748 ± 0.005	0.754 ± 0.018; 2.25 ± 0.21
10-125-10	0.468 ± 0.001	0.455 ± 0.003; 3.77 ± 0.15
5-125-20	0.473 ± 0.002	0.434 ± 0.004; 3.82 ± 0.21

^a The first number indicates compatibilizer content in wt% of PE, the second number indicates blending temperature (°C), and the third number indicates blending duration (min).

^b 95% Confidence interval of the parameter based on a count of >250 particles from one blend.

Table 4

Viscosity ratio, capillary numbers, and Taylor's minimum drop size for 9:1 PS-PE blends outlined in Section 2.2.1.

Code ^a	Viscosity ratio	Ca _c	Ca	D _T , nm
0-175-10	0.61	0.11	50.3	8.8
5-175-10	0.61	0.11	42.9	8.8
10-175-10	0.61	0.11	45.8	8.8
5-175-20	0.61	0.11	43.1	8.8
0-150-10	0.69	0.09	74.8	6.0
5-150-10	0.69	0.09	65.9	6.0
10-150-10	0.69	0.09	43.2	6.0
5-150-20	0.69	0.09	38.9	6.0
0-125-10	0.75	0.08	46.7	3.7
5-125-10	0.75	0.08	93.5	3.7
10-125-10	0.75	0.08	58.5	3.7
5-125-20	0.75	0.08	59.1	3.7

^a See Table 3 for codes.

(compatibilizer content, blend temperature/viscosity ratio, and blend time) indicated that decreasing the blend temperature, which would increase the PE/PS viscosity ratio resulted in the reduction of the particle size ($p = 0.018$). This is in concurrence with results reported by Favis and Chalifoux [42], Rumscheidt and Mason [43], and Serpe et al. [44] where a viscosity ratio approaching unity typically resulted in finer particles.

The addition of the block copolymer compatibilizer was expected to reduce the interfacial tension between the two immiscible polymers, which would theoretically decrease the droplet size of the dispersed phase leading to smaller particles [45,46]. However, the addition of the compatibilizer did not result in a significant ($p < 0.05$) change in particle size under the conditions used in this study. Horák et al. suggest that this discrepancy is possibly attributed to different procedures and evaluation methods used in the different studies, especially when compatibilizers with differing architectures are involved [47]. In addition, the efficiency of a particular block copolymer for reducing the size of particles varies between different pairs of homopolymers [48]. In this case, the effect of Kraton G® 1650E on the interfacial tension between the homopolymers used in this study and other pairs of homopolymers reported in the literature results in different droplet breakup characteristics, which leads to the variation in the particle size distribution.

The effect of the blending durations used in this study was also found to be irrelevant and did not have a significant effect ($\alpha = 0.05$) on the morphology or final particle size of the dispersed phase in the immiscible blends. It has been shown that the morphology and particle size are invariants of time for batch mixers due to a rapid establishment of equilibrium between droplet breakup and coalescence [49,50].

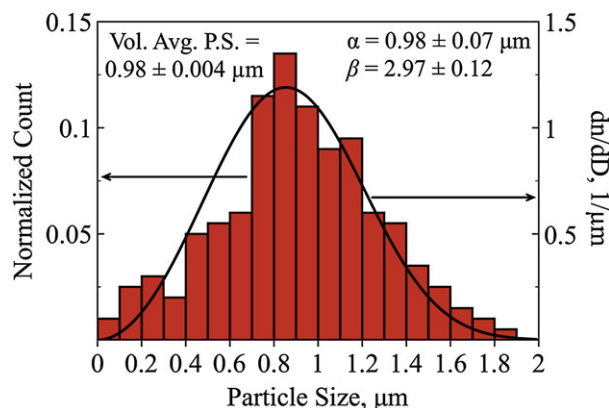


Fig. 2. Particle size distribution for PE particles extracted from sample 0-125-10.

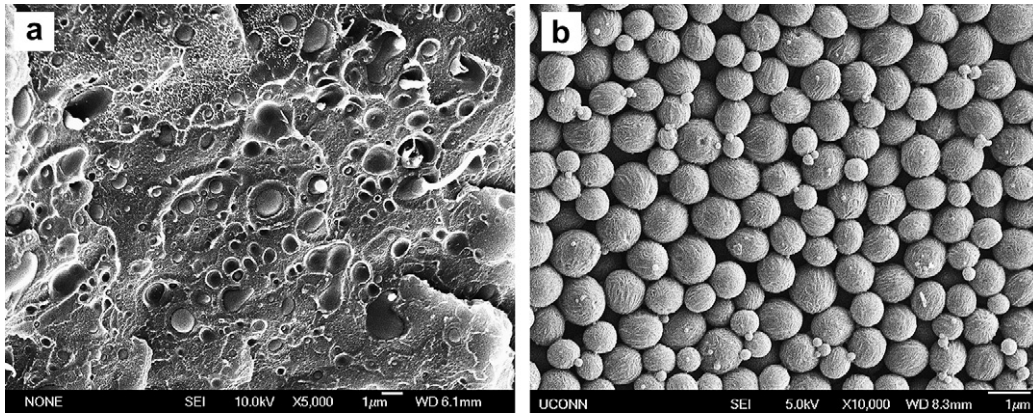


Fig. 3. SEM images of PE particles from sample 5-150-10 prepared using the method outlined in Section 2.2.1. (a) The PE particles still embedded in the PS matrix. A few of the PE particles were elongated during the cryogenic cracking process as can be seen in (a). (b) The same PE particles once extracted from the PS matrix using THF as a solvent for the PS.

Due to the high shear rate applied, Ca values much larger than the Ca_c were obtained indicating that the system had not reached a steady state, or the elastic forces were sufficient to prevent particle breakup. Since the flow in the mixer used in this study is a combination of simple shear and extensional flow, the calculated Ca_c values would predict the upper limit of the particle size [14]. Using Taylor's relation for the maximum particle size, D_T that would be stable under a simple shear flow of a Newtonian fluid,

$$D_T = \frac{4\Gamma(\eta_r + 1)}{\dot{\gamma}\eta_m(\frac{19}{4}\eta_r + 4)} \quad (4)$$

the expected particle sizes would be two decades lower in size than those shown in Table 4. However, Taylor's relation is only valid for small deformations in Newtonian-fluid mixtures and hence, may account for the discrepancy between the calculated and observed particle sizes. In addition, the Newtonian basis of the Ca_c does not take into account the viscoelastic effects of the polymers. The high elasticity of the PE melt suppresses the effect of the shear stress, which may suppress further droplet breakup beyond a certain point.

The larger-than-predicted particle size could also be explained by coalescence of the droplets during mixing. The combination of high droplet concentrations and shear rates increases the probability of droplet collision and film drainage, resulting in a limiting droplet size [37,51,52]. Most industrial blends and the majority of work reported in literature utilize formulations with a dispersed phase concentration that is typically $\geq 5\%$. Sundararaj and Macosko however, suggest that only blends with dispersed phase concentrations $\leq 0.5\%$ are independent of concentration effects [37]. Roland and Böhm also found that with increasing shear rates in their system, which would decrease coalescence [37,52], actually increased the amount of coalescence and consequently, the particle size.

3.2. Particle morphology and chemical composition

Fig. 3 shows SEM images of sample 5-150-10 produced using the method outlined in Section 2.2.1 before and after their recovery from the PS matrix following the blending and crosslinking procedure. The PE particles can be seen scattered independently

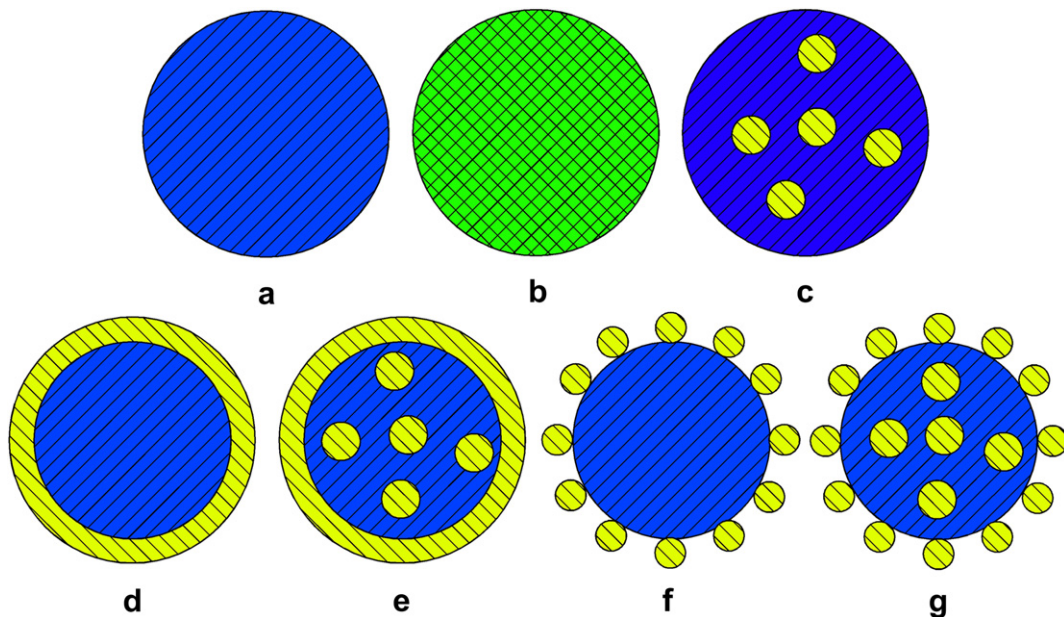

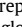
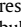


Fig. 4. Hypothesized structures of PE particles after recovery from the PS-PE blend with  representing the PS phase,  the PE phase, and  a PS and PE mixture. The addition of the compatibilizer is hypothesized to result in the formation of either a PS corona or surface globules as seen in particles d-g. There is also a possibility of PS microdomains forming within the PE particles during blending as seen in particles c, e, and g.

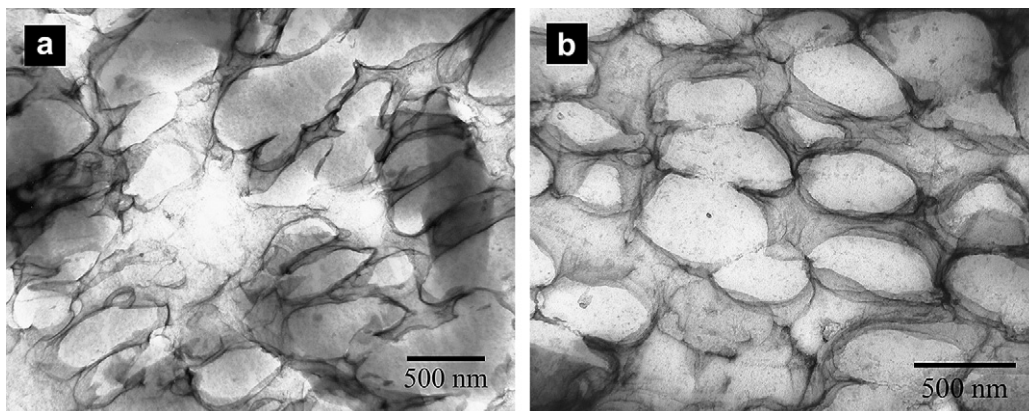


Fig. 5. TEM images of PE particles from samples (a) 0-150-10 and (b) 5-150-10. The dark regions surrounding the PE particles are due to the preferential OsO_4 staining of PS [54]. The density gradients in the matrix are due to uneven sample thicknesses while the elliptical shape of the PE particles are due to compression during the sectioning process.

and statistically in the PS matrix in Fig. 3a prior to recovery. Images of other samples prepared using this method were of similar morphology and hence, have been omitted for brevity.

Fig. 4 illustrates the possible structures of the PE particles with and without the addition of the block copolymer compatibilizer. With the addition of excess compatibilizer, a PS-rich shell could form, encapsulating the PE particle completely as depicted in Fig. 4d and e, whereas PE particles made with a compatibilizer concentration below the saturation limit could result in structures as depicted in Fig. 4f and g, where the PS blocks form independent globules on the surface of the PE particles due to their low number density. Particles made without the compatibilizer on the other hand, could result in corona-free structures as depicted in Fig. 4a and b. Another consequence of the addition of the block copolymer compatibilizer is the formation of microdomains comprising block copolymer micelles, which may form independently in the PS matrix phase or in the PE particles as illustrated in Fig. 4c, e, and g.

Hlavatá et al. have pointed out that the formation of the PS interfacial layer and microdomains is largely dependent on the molar mass of the styrene blocks of the compatibilizer [53]. If the length of these styrene blocks is on the order of magnitude or larger than the PS homopolymer chain, they would co-entangle causing them to be trapped in the PS matrix as small independent satellite particles. This would result in a mixture of pure PE particles (Fig. 4a) and smaller particles comprising the block copolymer micelles. On the other hand, if the PS block lengths are lower than the PS homopolymer chain, the block copolymer compatibilizer will migrate to the interface of the blend constituents, stabilizing any

structures formed resulting in a PS-rich corona or surface globules (depending on the concentration) as illustrated in Fig. 4d–g. For the case where the length of the styrene blocks falls below a critical limit and the length of the aliphatic block matches that of the aliphatic homopolymer in the blend, block copolymer micelles may form exclusively within the PE particles or in conjunction with a PS interfacial layer as illustrated in Fig. 4c, e, and g respectively.

Fig. 5 shows TEM images of PE particles from samples 0-150-10 and 5-150-10. The OsO_4 staining revealed PS-rich shells on both samples 0-150-10 and 5-150-10, which was not expected. We had hypothesized that the PE particles produced without the block copolymer would be free of a PS interfacial layer as described above. However, it appears that there is a residual amount of PS coating the surface of the PE particles made with and without the compatibilizer. It is possible that this coating is due to inadequate washing of the PE particles during the PS matrix extraction process. The possibility of PS inclusions within the PE particles as suggested in Fig. 4c, e, or g appear to be absent based on the lack of dark fields within the PE particles as seen in the TEM images.

Samples produced using the method outlined in Section 2.2.2 were mainly co-continuous and fibrous, aside from sample DCP01K as shown in Fig. 6. The addition of the block copolymer compatibilizer in this particular case did have an effect in reducing coalescence, as the resulting PE phase was less fibrous when compared to equivalent blends without the presence of the compatibilizer. The generally fibrous and co-continuous phase associated with this method can be attributed to the long residence time of the peroxide in the blend [55]. Since the PE is primed with the peroxide (via melt

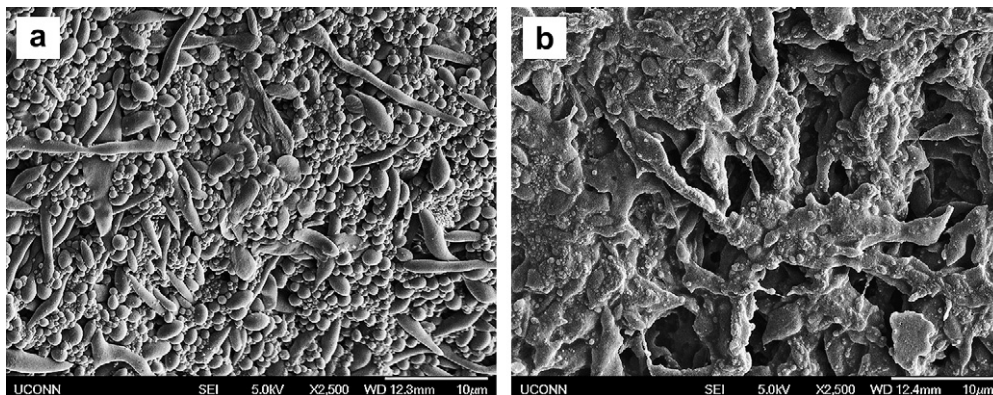


Fig. 6. SEM images of 9:1 PS-PE blends prepared using the method outlined in Section 2.2.2. PE once extracted from the PS matrix using THF as a solvent for the PS. Sample DCP01K (a) was the only formulation that resulted in discrete particles (spherical and rod-like) while the rest of the formulations resulted in a co-continuous fibrous phase (b).

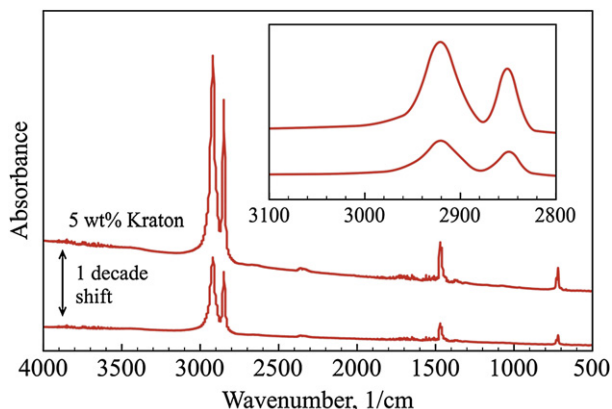


Fig. 7. FTIR spectra of crosslinked PE particles developed using the method outlined in Section 2.2.1 with and without the presence of the block copolymer compatibilizer. The inset plot is an enlargement of the spectra within the limits of 3150 and 2950 cm^{-1} .

blending) before the actual blends are made with PS, it is conceivable that the PE is slightly crosslinked despite the initial addition of a small amount of an antioxidant. This shifts the dynamic equilibrium between droplet breakup and coalescence of the PE phase in favor of coalescence during later blending.

Results from FTIR analysis on samples 0-150-10 and 5-150-10 (Fig. 7) were in concurrence with the TEM observations, indicating that both samples contained a small amount of PS with sample 5-150-10 containing more PS due to the addition of the block copolymer compatibilizer. Using a calibration curve (Fig. 8) derived from PE-PS blends with varying PS content, the PS contents for samples 0-150-10 and 5-150-10 were predicted and are shown in Table 5. The area under the 3030 cm^{-1} peak corresponding to the C-H stretching vibrations of the aromatic ring was used as a measure of PS content after normalizing for the sample thickness.

The theoretical PS content due to the addition of the block copolymer compatibilizer would be 1.5 wt% if all the chains were located either on, or within the PE particles. This value is less than the estimated saturation limit of 13.5–23.8 wt% for the largest and smallest particles respectively. The estimated saturation limit is based on ideal PS chains with the radius of gyration of the compatibilizer's PS block forming Gaussian coils arranged in a square array on the particle surface. Under these conditions, the PE particles would have a PS corona with a thickness of approximately 20 nm.

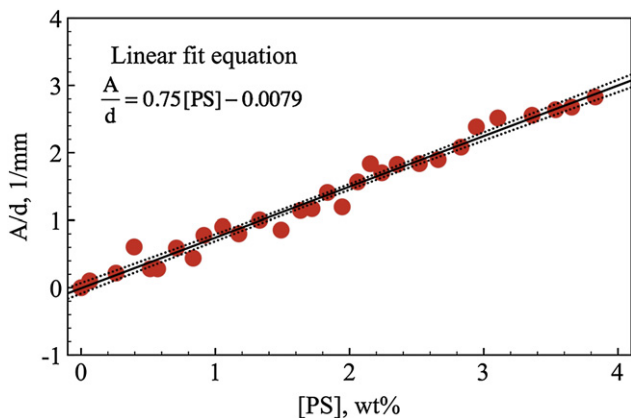


Fig. 8. PS calibration curve with 90% confidence bands for FTIR analysis of PE-PS blends using a Nicolet Magna-IR 560 Spectrometer. The ordinate represents the absorbance value normalized for film thickness while the abscissa is the concentration of PS in the PE-PS blends. The absorbance values were baseline corrected using the spectra of neat PE.

Table 5

PS content of samples 0-150-10 and 5-150-10 based on theoretical calculations and FTIR calibration curve.

Sample	$[\text{PS}]_{\text{saturation}}$, wt%	$[\text{PS}]_{\text{theoretical}}$, wt%	$[\text{PS}]_{\text{FTIR}}$, wt%
0-150-10	0	0	6.0×10^{-3}
5-150-10	13.6	1.5	8.0×10^{-2}

Results from the FTIR measurements indicate, however, that only a small fraction of the PS either from the block compatibilizer or from the homopolymer remained on the PE particles after extraction from the blend, which is much less than either the saturation limit or the calculated theoretical content.

This discrepancy is likely due to the block copolymer preferentially migrating into the PS phase leaving trace amounts of PS on the PE particles. These low concentrations (below saturation limits) would then possibly lead to structures such as depicted in Fig. 4f and g. High-magnification SEM images (Fig. 9) of these particles show the presence of ridges on the surface, which could be the result of PS surface globules stringing, forming sunflower-like structures as reported by Wang et al. [29]. These ridges are absent from particles made without the block compatibilizer copolymer.

In addition, FTIR analysis in Attenuated Total Reflection (ATR) mode was used to detect the presence of PS on the surface of the PE particles made with and without the block copolymer compatibilizer. However, the results indicated that both PE particle preparations yielded particles with no detectable PS on the surface. This is contrary to the results from other characterization techniques. This result is probably due to the limitations in the detection range of our instruments and not due to the absence of PS on the surface of the PE particles.

Results from the liquid-state ^1H NMR experiments were inconclusive, as the spectra only partially resembled those of neat PS. The ^1H NMR spectra of PE particles produced with and without the block copolymer compatibilizer, along with the spectra of neat PS are shown in Fig. 10. Although there is a small peak at 7.1 ppm in Fig. 10a corresponding to the aromatic protons in the *meta* and *para* positions of a styrene ring, the lack of a peak corresponding to the *ortho* protons at 6.5 ppm raises doubts concerning the presence of PS [56]. Following the same reasoning and discounting the absence of the *ortho* proton peak, it appears that the PE particles produced without the block copolymer compatibilizer possess residual PS as well (Fig. 10b), which is in agreement with the FTIR and TEM results.

Solid-state ^{13}C NMR results also indicate that both PE particles produced with and without the block copolymer compatibilizer contained a small amount of residual PS. The small broad peak

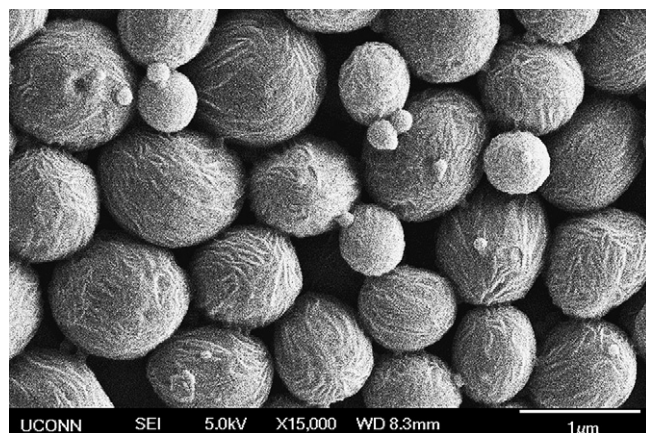


Fig. 9. High-magnification SEM image of sample 5-150-10 exhibiting PS ridges on the surface of the PE particles.

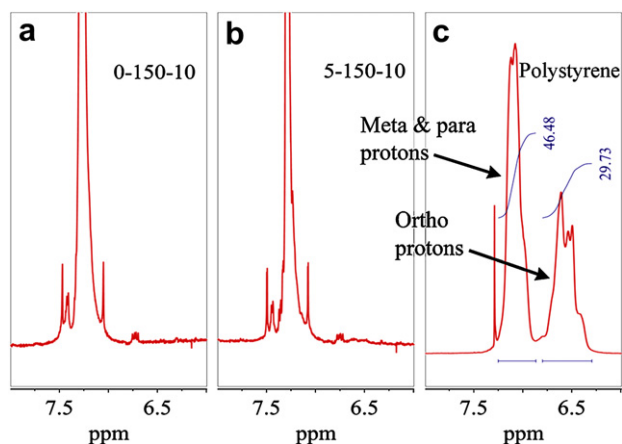


Fig. 10. Liquid-state ^1H NMR spectra of PE particles with (a) and without (b) the presence of the block copolymer compatibilizer. The ^1H NMR spectrum of neat PS is shown in (c) for reference.

comprising two components at 146 and 127 ppm in Fig. 11 indicates the presence of quaternary and protonated aromatic carbons, respectively [57]. Fig. 12a and b show the solid-state ^{13}C NMR spectra of PE and PS, respectively, for reference. However, the results do not provide sufficient information regarding the chemical composition of the particles and it is therefore not possible to conclude that PS forms a corona encapsulating the surface of the PE particles. There is a possibility of PS microdomains forming within the PE particles (Fig. 4c and d), especially in the case where the block copolymer compatibilizer is present [53]. Additionally, the high processing temperatures and shear rates may cause PS degradation fragments to dissolve in the PE phase, resulting in PS-infused PE particles (Fig. 4b). Somani and Shaw measured the miscibility of PS in PE using melt titration and determined that up to 0.13 wt% of PS with a molecular weight of 4000 g/mol may dissolve in PE [58]. Additionally, approximately 4.6×10^{-4} wt% of PS would dissolve in PE even if the PS used (222,000 g/mol) did not degrade during the blending process.

TGA results showed a difference in the onset of degradation between samples 0-150-10 and 5-150-10 with the latter degrading approximately 5 °C earlier than the former as shown in Fig. 13. As PS degrades at a lower temperature (404 °C) than PE (456 °C), the

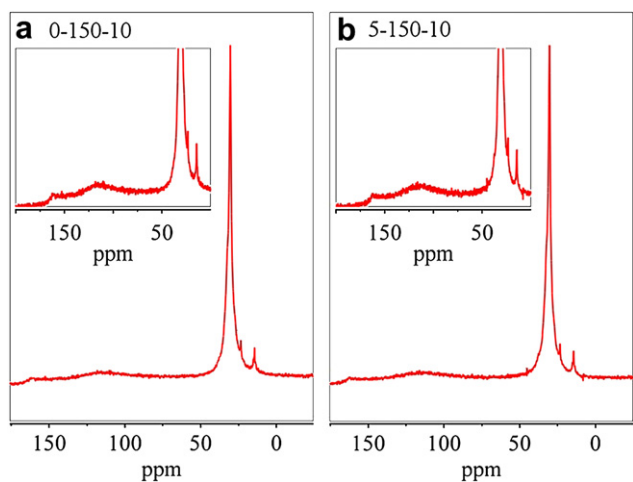


Fig. 11. Solid-state ^{13}C NMR spectra of PE particles with (a) and without (b) the presence of the block copolymer compatibilizer. The inset plot is an enlargement of the spectra within the limits of 175 and -25 ppm.

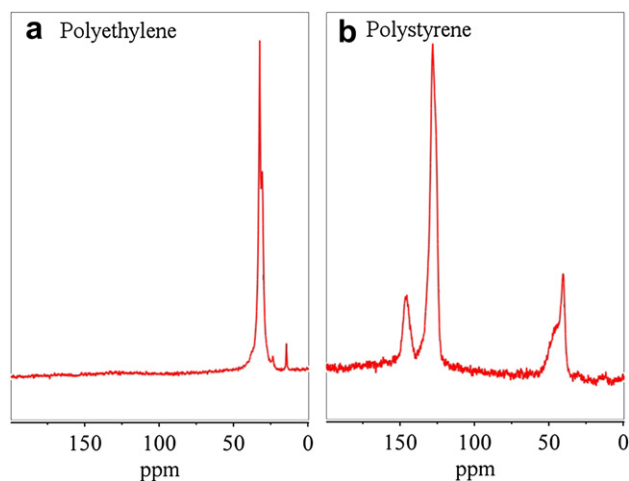


Fig. 12. Solid-state ^{13}C NMR spectra of neat PE (a) and PS (b).

earlier onset and higher rate of degradation exhibited by sample 5-150-10 in Fig. 13b and a respectively, suggests that the PS is very likely to be localized on the surface of the particles. The lower offset in degradation characteristics of both PE particle samples and that of neat PE is possibly due to thermal degradation of the PE phase during the blending process. As expected, the degradation characteristic of the block copolymer compatibilizer is a combination of its two constituents, namely PE and PS.

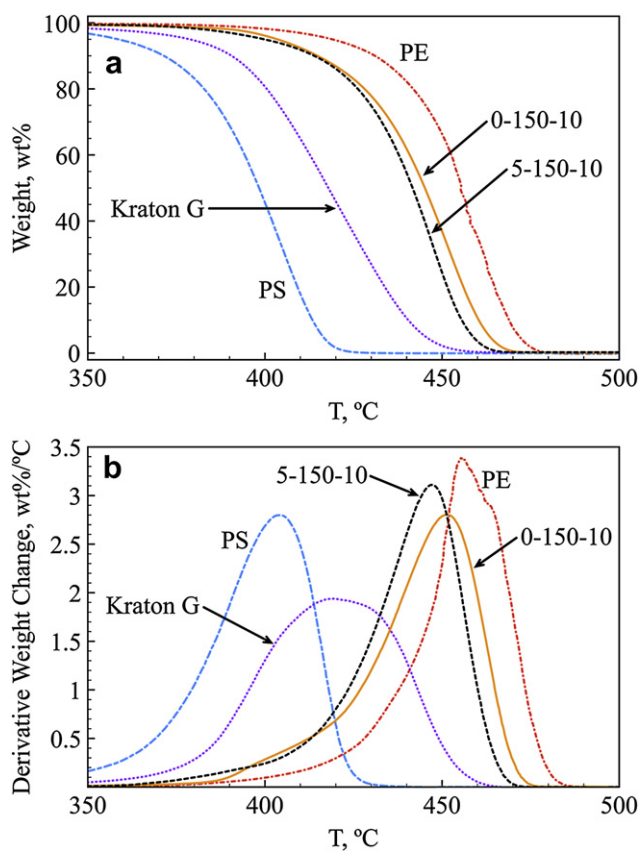


Fig. 13. TGA weight and derivative weight change of PS, PE, Kraton G[®] 1650E, 0-150-10, and 5-150-10 with temperature. Four separate and independent thermal scans (95% confidence interval of ± 3.4 °C) were performed for each sample. Only one scan is shown for the sake of clarity.

4. Conclusions

Crosslinked PE microparticles were successfully fabricated in an internal batch mixer using immiscible blends of PE and PS, which were crosslinked via electron-beam irradiation. The effect of the processing conditions and the addition of a block copolymer compatibilizer on the morphology and size distribution of the particles were studied and it was determined that only the decrease in blend temperature played a significant role in reducing the final size of the PE particles. The process involving in-situ crosslinking resulted in predominantly co-continuous PE phases and ellipsoidal structures while the method utilizing an electron beam as a cross-linking agent resulted in more uniform and spherical PE particles. The particles ranged from 0.374 ± 0.001 to 0.944 ± 0.003 μm , with the Weibull distribution function providing an adequate description of the particle size distribution.

The chemical composition of the recovered PE particles varied only slightly with and without the addition of the block copolymer compatibilizer. In both cases, there was always a residual amount of PS detected. This is contrary to our initial hypothesis of having a PS coating on the surface of the PE particles only when the block copolymer compatibilizer was used and having PE particles free of PS when no compatibilizer was used. PE particles produced with the compatibilizer had a lower PS content than expected while PE particles produced without the compatibilizer exhibited trace amounts of PS. This was confirmed using FTIR and NMR spectroscopy along with TEM image analysis. The trace amounts of PS found on the latter PE particles could be due to inadequate washing during the particle recovery step. However, environmental contamination during sample preparation and handling could also be responsible for the trace amounts of aromatics and should not be discounted.

It was found that the addition of the compatibilizer resulted in PE particles with a PS content of 0.08 wt% while formulations lacking the compatibilizer resulted in a PS content of 0.006 wt%. These values far underestimate the calculated saturation limit and theoretical content of 13.6 and 1.5 wt% respectively.

Although it was established that PS was present in both PE particles produced with and without the block copolymer compatibilizer, our results thus far failed to pinpoint the exact location of PS on the PE particles. Based on the information currently available, it is likely that the PS is confined to the outside of the PE particles. However, the possibility of it forming inclusions within the PE phase or dissolving slightly with PE cannot be completely dismissed. Work currently in progress to further decipher this issue include rheological and atomic force microscopy experiments, which would indirectly probe the surface of the PE particles and hopefully provide more information on the surface morphology of these particles.

Acknowledgements

We would like to extend our gratitude to Jeff Schroeder and Edith Rea (formerly) at General Cable (Willimantic, CT) for their help with the radiation crosslinking of the samples.

References

- [1] Funke W, Bauer H, Joos B, Kaczun J, Kleiner B, Leibelt U, et al. *Polym Int* 1993; 30(4):519–23.
- [2] Kihara N, Kanno C, Fukutomi T. *J Polym Sci Part A Polym Chem* 1997;35(8): 1443–51.

- [3] Antonietti M, Bremser W, Schmidt M. *Macromolecules* 1990;23(16):3796–805.
- [4] Ling GH, Shaw MT. *Polym Eng Sci* 2008;48(2):329–35.
- [5] Ling GH, Shaw MT. Thermo-gelation of surface-modified polyethylene microgels from fragmentation and immiscible blends. In: 15th international congress on rheology. Monterey, CA: American Institute of Physics; 2008. p. 1027.
- [6] Hong Z, Shaw MT, Weiss RA. *Macromolecules* 1998;31(18):6211–6.
- [7] Minale M, Mewis J, Moldenaers P. *AIChE J* 1998;44(4):943–50.
- [8] Mighri F, Carreau PJ, Aiji A. *J Rheol* 1998;42(6):1477–90.
- [9] Milliken WJ, Leal LG. *J Non-Newtonian Fluid Mech* 1991;40(3):355–79.
- [10] Vinckier I, Moldenaers P, Mewis J. *J Rheol* 1997;41(3):705–18.
- [11] Taylor GI. The formation of emulsions in definable fields of flow. *Proc R Soc Lond Ser A* 1934;146:501–23.
- [12] Taylor GI. The viscosity of a fluid containing small drops of another fluid. *Proc R Soc Lond Ser A* 1932;138:41–8.
- [13] Acrivos A. The breakup of small drops and bubbles in shear flows. In: 4th Annual New York academy of science international conference on physico-chemical hydrodynamics, vol. 404; 1983. p. 1–11.
- [14] Bentley BJ, Leal LG. *J Fluid Mech* 1986;167:241–83.
- [15] Grace HP. *Chem Eng Commun* 1982;14(3):225–77.
- [16] Rallison JM. *Annu Rev Fluid Mech* 1984;16:46–66.
- [17] de Bruijn RA. Deformation and breakup of drops in simple shear flow. Ph.D. thesis, Eindhoven University of Technology, Eindhoven, The Netherlands; 1989.
- [18] Meijer HE, Janssen JM. Mixing of immiscible liquids. In: Tadmor Z, editor. *Mixing and compounding of polymers: theory and practice*. Munich: Hanser Gardner Publications; 1994.
- [19] Galloway JA, Jeon HK, Bell JR, Macosko CW. *Polymer* 2005;46(1):183.
- [20] Lyu S, Jones TD, Bates FS, Macosko CW. *Macromolecules* 2002;35(20):7845–55.
- [21] Galloway JA, Koester KJ, Paasch BJ, Macosko CW. *Polymer* 2004;45(2):423.
- [22] Hong S, Bushelman AA, MacKnight WJ, Gido SP, Lohse DJ, Fetters LJ. *Polymer* 2001;42(13):5909.
- [23] Moon D, Kwon M, Park O. *Korean J Chem Eng* 2001;18(1):33.
- [24] Plochocki AP, Dagli SS, Curry JE, Starita J. *Polym Eng Sci* 1989;29(10):617–24.
- [25] Starita J. Microstructure of melt-blended polymer systems. Ph.D. thesis, Chemical Engineering, Princeton University, Princeton, NJ; 1970.
- [26] Tang W, Tang J, Yuan H, Jin R. *J Polym Sci Part B Polym Phys* 2007;45(16):2136–46.
- [27] Mekhilef N, Favis BD, Carreau PJ. *J Polym Sci Part B Polym Phys* 1997;35(2): 293–308.
- [28] Wang D, Sun G, Chiou B-S. *Macromol Mater Eng* 2007;292(4):407–14.
- [29] Wang D, Sun G, Chiou B-S. *Macromol Mater Eng* 2008;293(8):657–65.
- [30] Wang D, Sun G, Chiou B-S, Hinstroza JP. *Polym Eng Sci* 2007;47(11):1865–72.
- [31] Nalaskowski J, Drelich J, Hupka J, Miller JD. *J Adhes Sci Technol* 1999;13(1):1–17.
- [32] Kageyama K, Tamazawa J-I, Aida T. *Science* 1999;285(5436):2113–5.
- [33] Li H, Ke Y, Hu Y. *J Appl Polym Sci* 2006;99(3):1018–23.
- [34] Givens SR, Gardner KH, Rabolt JF, Chase DB. *Macromolecules* 2007;40(3): 608–10.
- [35] Goodrich JE, Porter RS. *Polym Eng Sci* 1967;7(1):45–51.
- [36] Chen R, Wu Q, Zhu F, Lin S. *J Appl Polym Sci* 2003;89(6):1596–605.
- [37] Sundararaj U, Macosko CW. *Macromolecules* 1995;28(8):2647–57.
- [38] Wang Z, Chan C, Zhu SH, Shen J. *Polymer* 1998;39(26):6801.
- [39] Gustafsson B, Boström JO, Dammert RC. *Angew Makromol Chem* 1998; 262(1):93–9.
- [40] GEO SC. DI-CUP® dicumyl peroxide vulcanizing agent and crosslinking agent. Technical information bulletin ORC-201M. Ambler, PA: GEO Specialty Chemicals, Specialty Additives Group.
- [41] Spurr AR. *J Ultrastruct Mol Struct Res* 1969;26(1–2):31.
- [42] Favis BD, Chalifoux JP. *Polym Eng Sci* 1987;27(21):1591–600.
- [43] Rumscheidt FD, Mason SG. *J Colloid Sci* 1961;16:238–61.
- [44] Serpe G, Jarrin J, Dawans F. *Polym Eng Sci* 1990;30(9):553–65.
- [45] Wu S. *Polym Eng Sci* 1987;27(5):335–43.
- [46] Velankar S, Van Puyvelde P, Mewis J, Moldenaers P. *J Rheol* 2001;45(4):1007–19.
- [47] Horák Z, Hlavatá D, Hromádková J, Kotek J, Hašová V, Mikešová J, et al. *J Polym Sci Part B Polym Phys* 2002;40(23):2612–23.
- [48] Appleby T, Cser F, Moad G, Rizzardo E, Stavropoulos C. *Polym Bull* 1994;32(4): 479.
- [49] Min K, White JL, Fellers JF. *J Appl Polym Sci* 1984;29(6):2117–42.
- [50] Schreiber HP, Olguin A. *Polym Eng Sci* 1983;23(3):129–34.
- [51] Elmendorp JJ, Van der Vegt AK. *Polym Eng Sci* 1986;26(19):1332–8.
- [52] Roland CM, Böhm GGA. *J Polym Sci Part B Polym Phys* 1984;22(1):79–93.
- [53] Hlavatá D, Horák Z, Hromádková J, Lednický F, Pleska A. *J Polym Sci Part B Polym Phys* 1999;37(14):1647–56.
- [54] Meyers GF, Grubb DT. *Polymer microscopy*. 3rd ed. New York: Springer; 2008.
- [55] Crevecoeur JJ, Nelissen L, van der Sanden MCM, Lemstra PJ, Mencer HJ, Hogt AH. *Polymer* 1995;36(4):753–7.
- [56] Baigl D, Seery TAP, Williams CE. *Macromolecules* 2002;35(6):2318–26.
- [57] Joseph Roychen, Ford Warren T, Zhang Shanmin, Tsyurupa MP, Pastukhov AV, Davankov VA. *J Polym Sci Part A Polym Chem* 1997;35(4):695–701.
- [58] Somani RH, Shaw MT. *Polym Eng Sci* 1984;24(8):601–7.